Applied Catalysis B: Environmental 310 (2022) 121303

Contents lists available at ScienceDirect

Applied Catalysis B: Environmental

journal homepage: www.elsevier.com/locate/apcatb

Highly stable and selective layered Co-Al-O catalysts for low-temperature CO_2 methanation

Zhihao Liu [a], Xinhua Gao [a,*], Bo Liu [a], Wenlong Song [a,b], Qingxiang Ma [a], Tian-sheng Zhao [a], Xu Wang [a,b], Jong Wook Bae [b], Xingjun Zhang [c], Jianli Zhang [a,*]

[a] State Key Laboratory of High-efficiency Utilization of Coal and Green Chemical Engineering, College of Chemistry & Chemical Engineering, Ningxia University, Yinchuan 750021, Ningxia, PR China
[b] School of Chemical Engineering, Sungkyunkwan University (SKKU), 2066 Seobu-ro, Jangan-gu, Suwon, Gyeonggi-do 16419 Republic of Korea
[c] Ningxia Academy of Metrology & Quality Inspection, National Quality Supervision and Inspection Center for Coal and Coal Chemical Products (Ningxia), Yinchuan 750200, PR China

ARTICLE INFO

Keywords:
CO_2 methanation
Co-based catalyst
Layered double hydroxide
Nanoparticle
Low temperature

ABSTRACT

A series of layered Co-Al-O catalysts derived from hydrotalcites for low-temperature CO_2 methanation were prepared via a hydrothermal method and reduced at 500, 550, 600, 650, and 700 °C, respectively. The characterisation results from XPS and CO_2-TPD revealed that the Co^0 content and basic sites over these catalysts were firstly increased and then decreased with the reduction temperature increasing, which led to the efficient dissociation of H_2 and CO_2 adsorption. *In situ* DRIFTS measurements revealed that the formation of CH_4 proceeded via the hydrogenation of carbonate and formate as intermediates. A superior catalytic performance of Co-Al-O-600 catalyst for CO_2 methanation was achieved with a CO_2 conversion of 74% and a CH_4 selectivity of 99% at low temperature of 250 °C. Moreover, it exhibited excellent resistance to coking and sintering upon a 240 h time on stream operation.

1. Introduction

Global warming and other manifestations of climate change caused by the emission of CO_2 upon fossil fuel combustion over the past few centuries require the research and development of CO_2 reduction technologies [1–3]. At present, the technologies can currently be divided into those based on CO_2 emission control, CO_2 capture and storage [4], and CO_2 capture and utilisation [5,6]. Technique of the first class requires the further development of existing technological processes to increase the efficiency of fossil energy usage and decrease CO_2 emission in chemical production process [7], whereas the second is disturbed of CO_2 leakage risk and high cost.

As for the third technology, the use of "green hydrogen" is the key point. Generally, the "green hydrogen" is produced by the electrolysis of water and the electricity power can ultimately be generated from renewable energy (RE). The hydrogenation of CO_2 as renewable, non-toxic, and abundant C1 resource with H_2 produced using RE is a promising research direction and the basic step of C1 chemistry [8]. Among the high-value-added products of catalytic CO_2 hydrogenation, e.g., CH_3OH, CO, HCOOH, CH_4, and hydrocarbons [9–13], CH_4 is an ideal energy carrier that can be transported by existing gas pipelines infrastructures. Additionally, the hydrogenation of CO_2 to CH_4, i.e., CO_2 methanation, allows one to address the insufficient market supply of CH_4 and is important for the coal-to-gas conversion, which is required for the clean utilisation of coal, and for the power-to-gas conversion, which is required for RE storage [14,15]. CO_2 methanation was first reported by Sabatier (Eq. (1)) [16] and is strongly exothermic, i.e., from the perspective of thermodynamics, CO_2 can be almost fully converted to CH_4 with a selectivity of ~100% under mild conditions [17].

$$CO_2(g) + 4H_2(g) \rightleftharpoons CH_4(g) + 2H_2O(g), \quad \Delta H_{298K} = -165 \text{ kJ mol}^{-1}. \qquad (1)$$

Traditional CO_2 methanation catalysts typically contain transition metals such as Co [18,19], Ni [20,21], Fe [22], Cu [23], Ru [24], Rh [25], and Pd [26]. Among them, noble metals (Ru, Rh, Pd) exhibit excellent catalytic performance but are poorly suited for large-scale industrial application because of their scarcity and high cost. Fe-based catalysts are typical Fischer-Tropsch catalysts with a wide product distribution, while Cu-based catalysts tend to promote carbon chain growth to produce high-carbon products [27,28]. The Ni-based CO_2

* Corresponding authors.
E-mail addresses: gxh@nxu.edu.cn (X. Gao), zhangjl@nxu.edu.cn (J. Zhang).

https://doi.org/10.1016/j.apcatb.2022.121303
Received 28 December 2021; Received in revised form 4 March 2022; Accepted 8 March 2022
Available online 12 March 2022

methanation catalysts are extensively studied because of high activity and relatively low price but are prone to coking and/or sintering at high reaction temperature and deactivation at low temperature due to the interaction of metal particles with CO and the formation of mobile Ni carbonyls [29]. Co catalysts are widely used in various CO_2 hydrogenation reactions like F-T reaction and methanol production for its excellent catalytic performance. Gordon et al. [30] studied hydrogenation of CO_2 on SiO_2-supported Group VIII metals, revealing that Co is more active than Ni in CO_2 methanation. As mentioned above, CO_2 methanation is thermodynamically favourable and reaches thermodynamic equilibrium even at low temperature [31], which allows one to decrease energy consumption and prevent the active species from coking or/and sintering. In addition, high temperatures favour the reverse water-gas shift reaction (RWGS) and thus increase the selectivity for CO and decrease that for CH_4 [17]. Moreover, as an eight-electron reduction reaction, CO_2 methanation may exhibit significant kinetic limitations at low temperature [2]. Therefore, current research focuses on the design of catalysts with high activities at low temperatures to overcome the kinetic energy barrier, e.g., Co supported on metal oxides and zeolites was reported to well promote low-temperature CO_2 methanation [32–34]. Feng et al. [33] reported Co/KIT-6 catalyst for CO_2 methanation and the catalyst showed an excellent performance with a CO_2 conversion of 48.9% and 100% CH_4 selectivity at 280 °C. Perez-Lopez et al. [34] investigated Co-Al mixed oxides derived from hydrotalcites for CO_2 methanation. The results indicated the Co66Al33 catalyst showed a highest CO_2 conversion of 56.1% at 400 °C, despite a period of stability. Song et al. [8] developed superior CO_2 methanation catalysts that Co supported on ZrO_2 and Al_2O_3. The Co/ZrO_2 catalyst showed high activity with CO_2 conversion of 92.5% and CH_4 selectivity of 99.9% without deactivation after 300 h TOS, but the reaction conditions are harsh with a high temperature and pressure of 400 °C and 3 MPa. That is, the simultaneous realisation of high CO_2 conversion, high CH_4 selectivity, and long lifetime at mild conditions remains a daunting task. CO_2 methanation requires the co-operation of the metal and the metal-support interface, which promote the dissociation of H_2 and the activation of CO_2, respectively [35]. Catalyst performance is affected by support properties such as pore size, structure, and interaction with metals [35,36] as well as by the reduction degrees of the metal oxide and the support. Zhou et al. [37] investigated the effect of reduction degree on catalyst performance, revealing that reduction temperature had a significant impact on specific surface area and active species content. By changing the reduction temperature, the authors prepared catalysts with different Co contents and, hence, different activities. Among the oxide supports, Al_2O_3 is the one most commonly used for methanation catalysts. Szanyi et al. [38] reported Al_2O_3-supported Pd as a CO_2 methanation catalyst, showing that Al_2O_3 played a crucial role in CO_2 adsorption and demonstrating that CO_2 reacted with the surface hydroxyl groups of Al_2O_3 to form bicarbonates, which were subsequently reduced to CH_4. Song et al. [13] reported that Al_2O_3 engaged in strong interactions with the supported metals and affected the dispersion and particle size of Fe-based catalysts. Su et al. [39] suggested that the main problem of Al_2O_3-supported catalysts is their poor water resistance, i.e., the facile inactivation of these catalysts by water, which is a main product of the methanation reaction.

Despite these efforts, there are still difficulties in realizing high CO_2 conversion and long lifetime at the same time, and the influence of reduction degree of the Co species has not been fully studied. In view of the above problems, suitable supports and effective immobilisation approaches are highly sought after. Recently, layered double hydroxides (LDH) have attracted attention as sorbents and heterogeneous catalysts because of their structural controllability and good hydrothermal stability [40,41]. Generally, catalysts prepared by impregnation suffer from rapid deactivation due to the sintering and/or aggregation of metal nanoparticles. In contrast, LDH-derived catalysts show good stability due to the anchoring effect of their support, and do not easily undergo active species sintering and/or aggregation [20]. Gray et al. [42] probed the structure of LDH and found that M^{II} and M^{III} cations in the hydroxide layers are arranged in a highly ordered manner. Duan et al. [43] reported that metal oxides or metal-metal oxide composites can be obtained by heating LDH in air or under reducing conditions. This approach allows one to prepare supported metal nanoparticle catalysts with specific morphology and good stability.

Herein, layered Co-Al-O catalysts derived from a Co-Al LDH were fabricated at different reduction temperatures and used for low-temperature CO_2 methanation, showing excellent activity and CH_4 selectivity at 250 °C. The optimal catalyst was prepared at 600 °C and was not deactivated upon 240-h operation at 250 °C, achieving a CO_2 conversion of 74% and a CH_4 selectivity of 99%. *In situ* diffuse reflectance infrared Fourier transform spectroscopy (DRIFTS) experiments revealed that CO_2 was sequentially converted into carbonates, formates, and, finally, CH_4, while the phase changes during catalyst synthesis were probed by *in situ* X-ray diffraction (XRD).

2. Experimental

2.1. Catalyst preparation

Co-Al LDH ($Co^{2+}/Al^{3+} = 3$) was synthesised hydrothermally. Co $(NO_3)_2.6\,H_2O$ (Sinopharm Chemicals; 8.73 g, 30 mmol) and Al $(NO_3)_3.9\,H_2O$ (Sinopharm Chemicals; 3.75 g, 10 mmol) were dissolved in deionised water (100 mL), and the solution was treated with urea (Sinopharm Chemicals; 18.02 g, 300 mmol) and stirred for 30 min. After stirring, the suspension was transferred into a Teflon-lined stainless-steel autoclave for 12-h hydrothermal treatment at 120 °C under autogenous pressure. The precipitate was filtered off, washed with deionised water until the pH of the washings reached 7, and dried at 80 °C overnight to obtain Co-Al LDH. Co-Al oxide was obtained by calcining Co-Al LDH in air at 400 °C for 4 h and was subsequently reduced in a flow of 10 vol% H_2/Ar (30 mL min^{-1}) for 3 h at 500, 550, 600, 650, or 700 °C to afford catalysts denoted as Co-Al-O-T (T = 500, 550, 600, 650, 700). Then, a flow of 1 vol% O_2/N_2 (25 mL min^{-1}) was introduced to passivate the catalysts for 1 h before characterisation and catalytic testing.

2.2. Characterisation

XRD patterns were recorded on a Rigaku D/MAX2200PC instrument at 40 kV and 40 mA using Cu K_α radiation ($\lambda = 0.154$ nm). The scan rate equalled 10° min^{-1}, and the scan range (2θ) equalled 5–80°. Changes in catalyst phase composition during the reduction process were probed by *in situ* XRD measurements, which were performed using Rigaku SmartLab instrument with Cu Kα radiation. The reducing gas was introduced into the reactor chamber from a rotameter for 30 min, and the heating rate of 5 °C min^{-1} was employed to reach the reduction temperatures. Low pressure was maintained in the reaction pool during the entire reduction process.

Textural properties were extracted from N_2 adsorption-desorption isotherms recorded at − 196 °C on a JW-BK132F instrument for samples that had been degassed at 350 °C for 6 h. Specific surface areas and pore size distributions were calculated using Brunauer-Emmett-Teller and Barrett-Joyner-Halenda methods, respectively.

Scanning electron microscope (SEM) images were obtained using a Hitachi S-4700 field emission SEM at 20 kV, with the surface of the samples coated with a thin gold layer to avoid a charging effect.

Morphology and microstructure were studied by high-resolution transmission electron microscopy (TEM; FEI Talos F200X) at an accelerating voltage of 200 kV. The samples were dispersed in ethanol and ultrasonicated for 30 min. Several drops of the resulting suspension were placed on a carbon-coated copper grid and dried at ambient temperature.

H_2 temperature-programmed reduction (H_2-TPR) profiles were recorded using a Micromeritics AutoChem II 2920 instrument to analyse

the reducibility of calcined catalysts. Typically, the calcined sample (0.05 g) was packed into the quartz tube, flushed with He (30 mL min^{-1}) at 350 °C for 1 h, and then cooled in He (30 mL min^{-1}) to 50 °C. Subsequently, the gas was switched to 10 vol% H_2/He (30 mL min^{-1}), and the temperature was raised to 800 °C at a rate of 10 °C min^{-1}.

CO_2 temperature-programmed desorption (CO_2-TPD) profiles were recorded using the equipment employed for TPR measurements. Typically, the catalyst (0.05 g) was pre-treated in 10 vol% H_2/He (30 mL min^{-1}) at a certain temperature for 1 h and then exposed to a flow of He (30 mL min^{-1}) at the same temperature for 0.5 h to achieve desorption. The samples were then cooled to 50 °C, exposed to a flow of 10 vol% CO_2/He (30 mL min^{-1}) for 1 h, and flushed with He (30 mL min^{-1}) for 0.5 h to remove physically adsorbed species. Finally, the samples were heated to 700 °C at a rate of 10 °C min^{-1}, and resulting profiles were obtained using thermal conductivity detector (TCD).

The chemical states of surface elements were probed by X-ray photoelectron spectroscopy (XPS), and the related measurements were performed on a ThermoFisher ESCALAB250 spectrometer equipped with a monochromatized Al K_α radiation source at an operating voltage of 12 kV and a current of 12 mA. Calibration was performed using the C 1 s peak at 284.6 kV. The acquired spectra were deconvoluted and background-corrected using XPSPEAK software.

Thermogravimetric analysis (TGA; TGA/SDTA851e Thermobalance) was conducted in the range of 30–800 °C at a heating rate of 10 °C min^{-1} in a flow of N_2 (30 mL min^{-1}).

In situ diffuse reflectance infrared Fourier transform (DRIFT) spectra were recorded on a Nicolet 6700 spectrometer equipped with a reaction unit using 50 scans and a resolution of 6 cm^{-1}. The sample was pressed into a disk, activated at 600 °C in 10 vol% H_2/He (30 mL min^{-1}) for 1 h. Then, the sample was cooled to 300 °C and scanned in a flow of Ar (30 mL min^{-1}) to obtain a background spectrum. Subsequently, the sample was exposed to the reaction gas of 20 vol% CO_2/H_2 (30 mL min^{-1}).

2.3. Catalytic performance test

CO_2 hydrogenation performance was tested in a pressurised micro fixed-bed reactor with an inner diameter of 6 mm. The catalyst (20–40 mesh, 0.2 g (~0.1 mL)) was placed into the reactor, and the feed gas (20 vol% CO_2/H_2) was introduced into the tube at a weight hourly space velocity of 5000 mL g^{-1} h^{-1} and a pressure of 2 MPa. All catalysts were evaluated at a relatively low temperature of 250 °C, and the most active catalyst was additionally evaluated at 300 °C to increase CO_2 conversion.

The reaction products were analysed by an on-line gas chromatograph (GC-9160). CO_2, CO, and CH_4 were detected by a thermal conductivity detector equipped with a carbon molecular sieve column. CO_2 conversion ($X(CO_2)$) and CH_4 selectivity ($S(CH_4)$) were calculated using the carbon-based normalisation of peak areas (Eqs. (2) and (3), respectively).

$$X(CO_2) = \frac{n_{CO2,in} - n_{CO2,out}}{n_{CO2,in}} \times 100\% \quad (2)$$

$$S\left(CH4\right) = \frac{n_{CH4,out}}{n_{CO2,in} - n_{CO2,out}} \times 100\% \quad (3)$$

where $n_{CO2,in}$ and $n_{CO2,out}$ are the molar concentration of CO_2 in the feed and effluent gas, respectively; $n_{CH4,out}$ is the molar concentration of CH_4 in the effluent gas.

3. Results and discussion

3.1. Crystalline structure

Fig. 1 and S1 presents the XRD patterns of various catalysts and their precursors, respectively. The pattern of Co-Al LDH in the Fig. S1 featured peaks at $2\theta = 11.3, 22.8, 34.5, 38.7, 46.2$ and $59.6°$ that were indexed to the (003), (006), (012), (015), (018) and (110) planes of the LDH structure, respectively [44]. After calcination in air, these peaks disappeared and were replaced by those of Co_3O_4 and/or $CoAl_2O_4/Co_2AlO_4$ spinels, at $2\theta = 31.2°$ (220), 36.8° (311), 44.8° (400), 59.3° (442), 65.2° (440) [34]. Considering that Co_3O_4 and mixed oxides spinels present similar diffraction peaks which appears to be overlapped, these phases cannot be distinguished through XRD. Fig. 1 presents the catalyst samples reduced at different temperatures, and it is clear that the dominant phases are CoO and Co. Specifically, peaks at $2\theta = 44.2°$ (111), 51.5° (200) and 75.8° (220) were ascribed to face-centred cubic Co, while those at $2\theta = 36.6°$ (111), 42.6° (200), and 61.8° (220) were assigned to CoO [45]. Meanwhile, the presence of CoO species also indicated that the mixed oxides spinels are difficult to be completely reduced. With increasing reduction temperature, the peaks of CoO lost intensity, whereas those of Co gained intensity, i.e., high temperature promoted the reduction of CoO to Co. The Co^0 content increased from 44.2% to 86.3% with the reduction temperature increasing from 500 ℃ to 700 ℃ as shown in Table 1. The high Co^0 contents indicated the enhanced reducibility and was identified as one of the reasons for the high activity and stability of the catalysts prepared herein.

The structural changes of Co species during reduction process were characterised by *in situ* XRD (Fig. 2). The intensity of characteristic peaks of Co_3O_4 and/or $CoAl_2O_4/Co_2AlO_4$ spinels observed at 25 °C became obviously weaker at 300 °C with the appearance of CoO, which indicated the reduction of Co_3O_4 to CoO. At 350 °C, a weak signal of Co metal appeared, and CoO and Co subsequently became the dominant phases. The diffraction peaks of Co metal gained intensity with gradually disappearance of Co-Al oxide, while the diffraction peak intensity of CoO first increased and then decreased with increasing temperature, indicating that the samples underwent a continuous reduction process. This result is also in line with the XRD results in Fig. 1. The reduction temperatures of Co_3O_4 and CoO observed herein were much lower than those observed for Co-Al oxide prepared by impregnation [8]. Thus, the LDH-derived Co-Al oxide showed good reducibility and a high reduction degree, both of which benefitted catalytic activity.

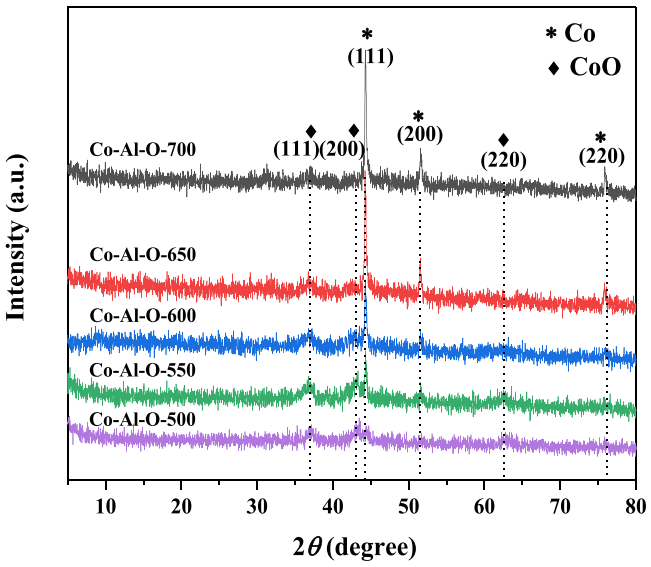

Fig. 1. XRD patterns of Co-Al-O catalysts reduced at different temperatures.

Table 1
Selected properties of the prepared catalysts.

Sample	surface area (m^2 g^{-1})	Pore size (nm)	Pore volume (cm^3 g^{-1})	Co particle size (nm)[a]	Co content (wt %)[b]	
					Co^0	CoO
Co-Al-O-500	107	6.1	0.23	17.50	44.2	55.8
Co-Al-O-550	100	6.3	0.22	24.58	67.2	33.0
Co-Al-O-600	85	6.8	0.20	26.88	67.8	32.2
Co-Al-O-650	57	7.4	0.15	28.15	79.7	20.3
Co-Al-O-700	37	8.6	0.12	33.87	86.3	13.7

[a] Calculated using the Scherrer equation.
[b] Calculated by integrating the XRD peak area.

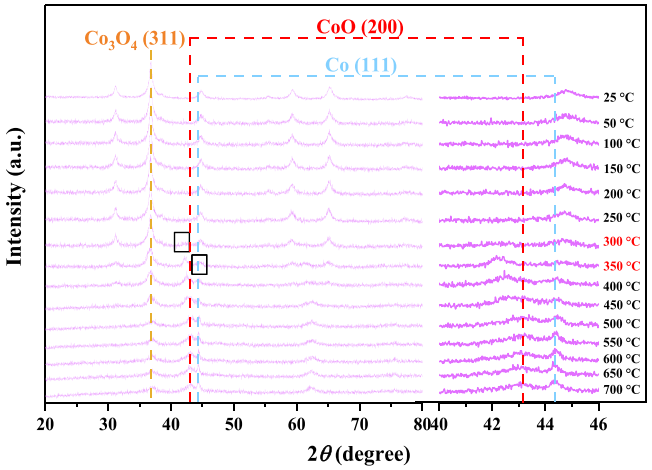

Fig. 2. *In situ* XRD patterns of Co-Al oxide recorded during reduction process.

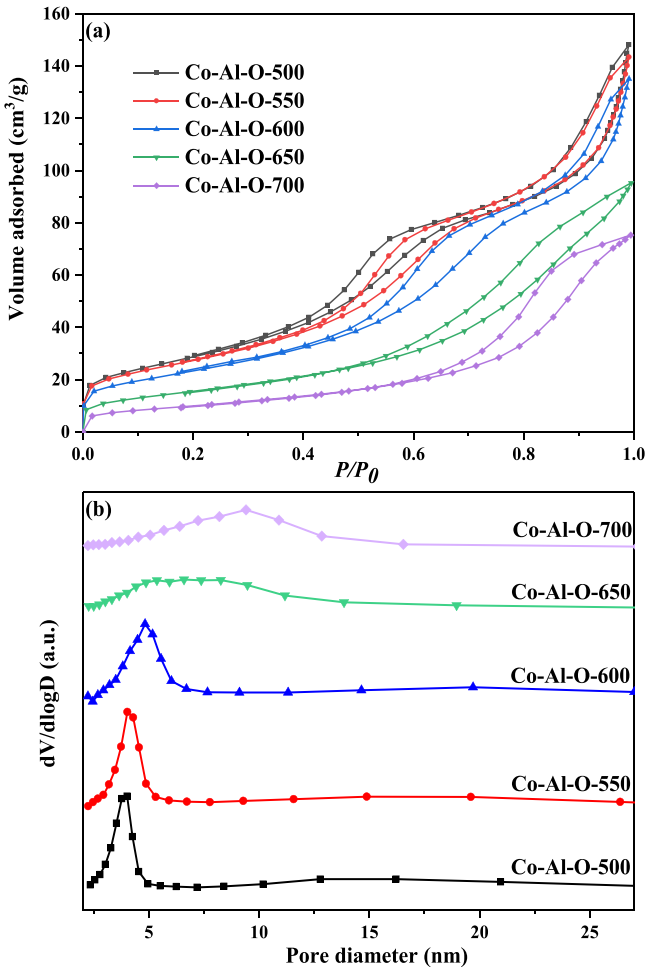

Fig. 3. (a) N_2 adsorption-desorption isotherms and (b) pore size distributions of the prepared catalysts.

3.2. Textural properties

Fig. 3 shows the N_2 adsorption-desorption isotherms and pore size distributions of the prepared samples, respectively, while the physical properties extracted from these isotherms are summarised in Table 1. All catalysts displayed type IV isotherms according to the IUPAC classification [46] and were therefore concluded to have mesoporous structures. The adsorption and desorption branches almost coincided at relatively low relative pressures, which was attributed to the monolayer adsorption of N_2 on mesoporous catalysts. At moderate relative pressures, the adsorption branches rose faster than desorption branches because of N_2 capillary condensation, which resulted in the appearance of hysteresis loops [47]. H2 hysteresis loops were observed for catalysts reduced below 650 °C, while H3 hysteresis loops were observed for catalysts reduced at 650 and 700 °C. The results indicated that samples reduced at 500, 550, and 600 °C featured typical mesoporous structures with narrow pore size distributions. At overly high reduction temperatures, these mesoporous structures were partly destroyed to afford wide pore size distributions (Fig. 5b) [37]. In addition, the condensation steps of Co-Al-O-650 and − 700 were shifted to higher relative pressures, which indicated that reduction temperature affected catalyst pore size [47]. At high relative pressures, the adsorption and desorption branches coincided, which was attributed to the multi-layer adsorption of N_2 on the catalyst surface.

Table 1 reveals that with increasing reduction temperature, the specific surface area and pore volume decreased, whereas the pore size increased. This behaviour was ascribed to the fact that high reduction temperatures can promote the reaction of Co species with the –OH groups on the support surface to form Co–OH moieties and thus partly block the pore structure and induce its reorganisation [48]. Moreover, physical properties are often related to the state of metal dispersion. High reduction temperatures favour the aggregation of Co species to form larger crystallites and thus reduce metal dispersion and decrease catalytic activity.

3.3. SEM analysis

Fig. 4 presents SEM images of Co-Al LDH, Co-Al oxide, and Co-Al-O-T catalysts. Co-Al LDH and Co-Al oxide contained typical flower-like nanosheet structures with a relatively uniform size distribution, which indicated the successful preparation of the LDH precursor and the retention of its structure upon calcination. All samples featured irregular slit holey structures due to the stacking of nanosheets and their mutual intercalation [49]. Co-Al-O-500, − 550, and − 600 inherited the layered structure of the precursor, which facilitated the high dispersion of Co nanoparticles. Meanwhile, these layered structures were partly damaged upon reduction at 650 and 700 °C, which indicated that high temperatures led to pore structure reorganisation, in line with the trend observed for specific surface area.

3.4. TEM analysis

Fig. 5 and S2 presents TEM images of the prepared catalysts, revealing that all samples exhibited a porous lamellar structure [40]. In addition, Co-Al-O-500, − 550 and − 600 showed uniform pore

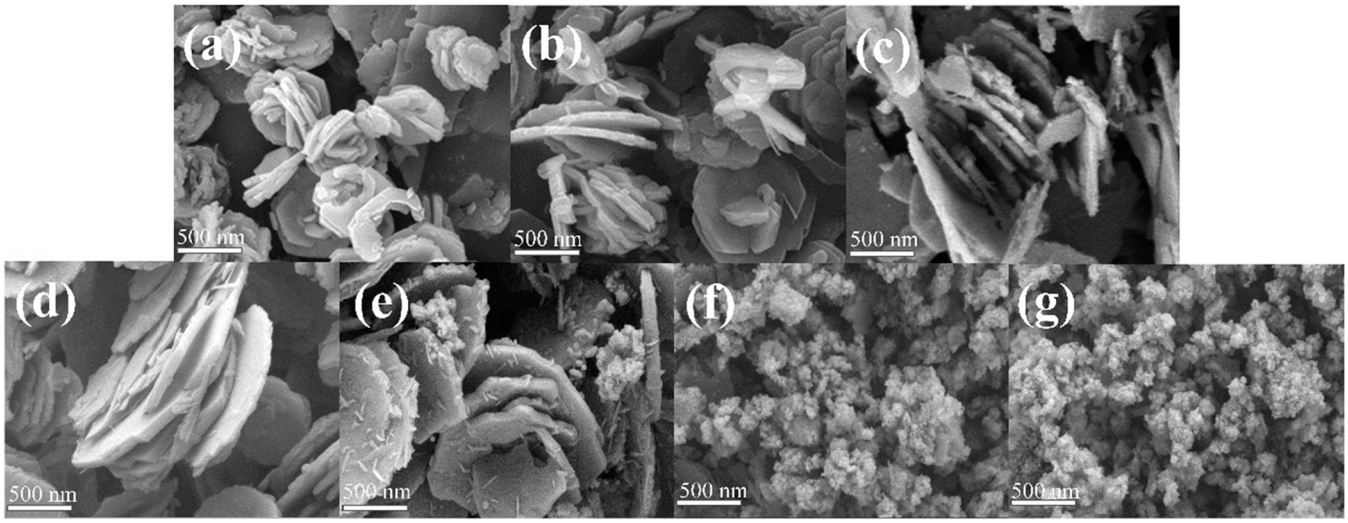

Fig. 4. SEM images of (a) Co-Al LDH, (b) Co-Al oxide, (c) Co-Al-O-500, (d) Co-Al-O-550, (e) Co-Al-O-600, (f) Co-Al-O-650, and (g) Co-Al-O-700.

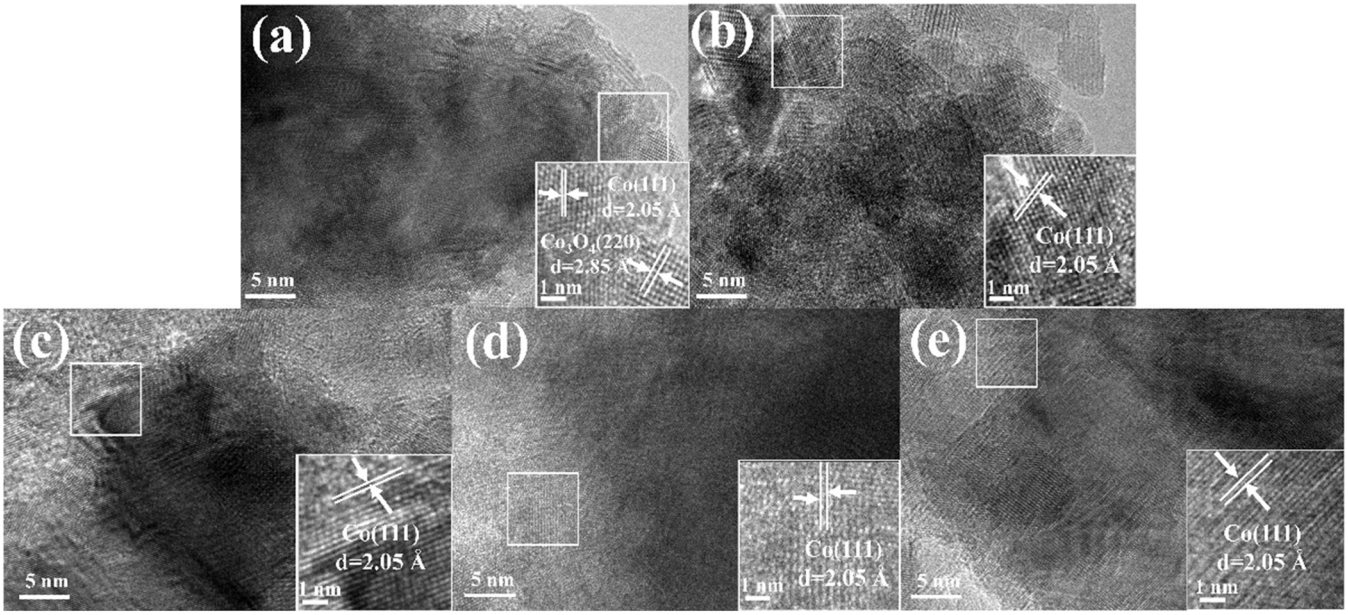

Fig. 5. TEM images of (a) Co-Al-O-500, (b) Co-Al-O-550, (c) Co-Al-O-600, (d) Co-Al-O-650, and (e) Co-Al-O-700.

structures and no obvious aggregation. Thus, at low reduction temperatures, the mesoporous structure of the support was not destroyed, and Co species were highly dispersed on the support. It was worth mentioning that there was a part of Co_3O_4 (220) in the Co-Al-O-500 catalyst even if it was not found in XRD results, indicating that the catalyst cannot be completely reduced at 500 °C. With increasing reduction temperature, these mesoporous structures were progressively destroyed, and the edges of the pore walls appeared irregular and ambiguous, which indicated that high reduction temperatures facilitate the aggregation of Co species to block pores. This result agreed with that of N_2 adsorption-desorption isotherm analysis. Fig. S3 presents the energy-dispersive X-ray elemental mappings of Co-Al-O-600, revealing that active Co species were successfully introduced into the Al_2O_3 support and that Co, Al, and O were uniformly dispersed.

3.5. Reduction behaviours of calcined catalysts

Fig. 6a and b present the H_2-TPR profiles of pure Co_3O_4, bare Al_2O_3 and Co-Al oxide, respectively. In Fig. 6a, the profile of bare Al_2O_3 showed no obvious peaks, while that of pure Co_3O_4 showed two peaks attributable to the reduction of surface and bulk Co_3O_4 species to Co [50]. The deconvolution of Fig. 6b using Gaussian functions was performed for a better analysis. The results showed that the profile of Co-Al oxide featured two distinct reduction peaks centred at 320 °C and 693 °C, respectively. The first one is related to the reduction of Co_3O_4, while the letter at higher temperatures corresponding to the reduction of mixed oxides spinels [34,51]. The deconvolution of the TPR profile revealed the presence of five reduction peaks. The peaks located in the first region (295 °C and 335 °C) are related to the continuous reduction of Co_3O_4 ($Co^{3+} \rightarrow Co^{2+} \rightarrow Co^0$). This result is also consistent with in-situ XRD data in Fig. 2. The peaks located at 690 °C and 720 °C in the second region can be attributed to the reduction of mixed oxides Co_2AlO_4 (inverse spinel) and $CoAl_2O_4$ (normal spinel), respectively [52]. The peak around 626 °C is ascribed to the reduction of a phase between Co_3O_4 and Co_2AlO_4 which is formed in samples with high Co/Al ratios [34].

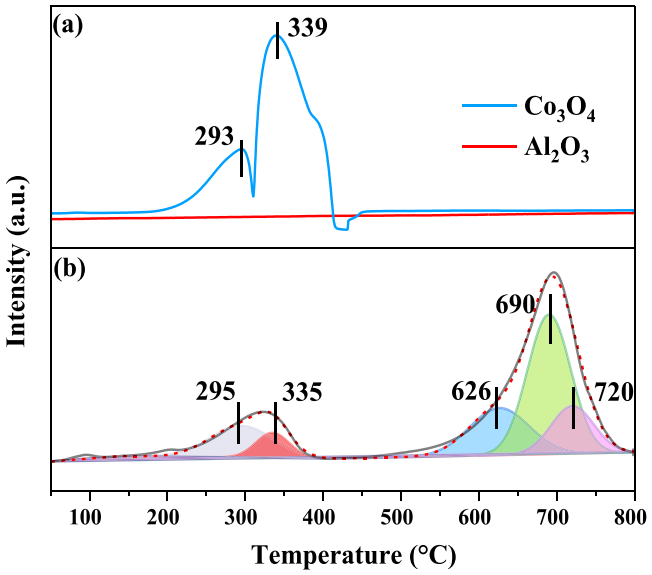

Fig. 6. H_2-TPR profiles of (a) pure Co_3O_4, bare Al_2O_3 and (b) Co-Al oxide.

3.6. CO_2-TPD analysis

Fig. 7 presents the CO_2-TPD profiles of the prepared catalysts, revealing the presence of three main peaks in the investigated temperature range and thus suggesting the presence of weakly, moderately and strongly basic CO_2 adsorption centres on the catalyst surface. The low total number of basic sites observed for samples reduced at high temperature was attributed to their low surface areas. Peak α was assigned to CO_2 desorption from hydroxyl groups related to bicarbonate species on the catalyst surface. The appearance of a shoulder peak due to CO_2 weakly absorbed on Co nanoparticles at higher reduction temperatures indicated that the samples were well reduced [53]. Peaks β and γ were attributed to CO_2 adsorbed at Lewis acid-base pairs on the catalyst surface and on O^{2-} species, respectively [54]. Previous studies have shown that CO_2 adsorbed at strongly basic sites is difficult to desorb for the subsequent reaction. Thus, the weak and medium basic sites bind CO_2 sufficiently strongly for its activation and subsequent reduction. The α and β peak area showed a trend of first increasing and then decreasing with the reduction temperature increasing and Co-Al-O-600 exhibited the highest density of weak and medium basic sites of 2.90 mmol g_{cat}^{-1}. More intense CO_2 desorption peaks and higher capacity indicate larger amounts of adsorbed CO_2 and CO_2 adsorption centres [55]. Therefore, we concluded that reduction temperature had a significant impact on CO_2 adsorption capacity and that Co-Al-O-600 featured the most basic and numerous CO_2 adsorption centres among the tested samples (Table 2).

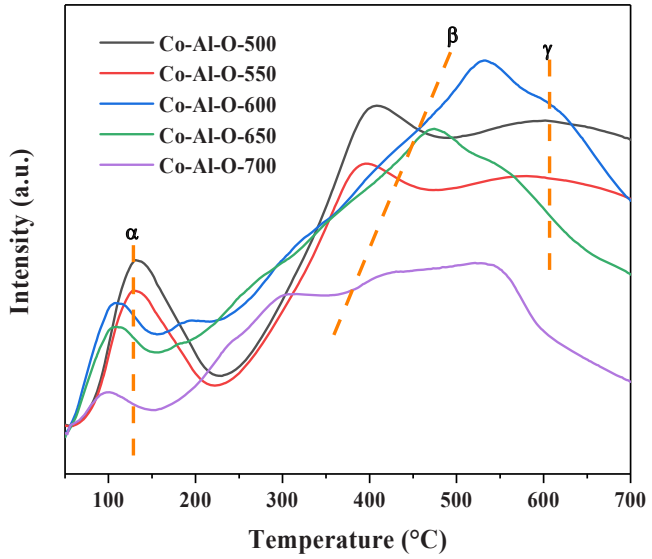

Fig. 7. CO_2-TPD profiles of the prepared catalysts.

3.7. XPS analysis

Fig. 8 presents the Co 2p spectra of the prepared catalysts, and the information extracted from these spectra is summarised in Table 2. All spectra featured two distinct peaks centred at 780.5 and 796.3 eV (Co $2p_{3/2}$ and Co $2p_{1/2}$ transitions, respectively [56]) along with two weak satellite peaks centred at 786.1 and 802.6 eV. The Co $2p_{3/2}$ peak was deconvoluted into the signals of Co^0 and Co^{2+} at 780.2 and 781.4 eV, respectively [57]. Moreover, the spin-orbital splitting (ΔE) values were similar to that of Co^{2+} species ($\Delta E = 16.0$ eV) in Table 2, and no obvious peaks corresponding to Co^{3+} were observed, which suggested that Co^{3+} in Co-Al oxide was fully reduced to Co^0 and Co^{2+} [57], in line with the results of XRD and H_2-TPR measurements.

For Co-Al-O-550, − 600, − 650, and − 700, the area of the Co^0 peak exceeded that of the Co^{2+} peak, whereas the opposite was true for Co-Al-O-500. This finding agreed with the relative contents of Co^0 and Co^{2+} listed in Table 2. The higher Co^0/Co^{2+} atomic ratio of Co-Al-O-600 indicated the better reducibility of this catalyst and further implied that Co^{3+} in the Co-Al oxide can be easily reduced to Co^0 at 600 °C. At a lower reduction temperature, Co^{3+} in the Co-Al oxide could not be effectively reduced to Co^0, which resulted in a high content of surface Co^{2+} in Co-Al-O-500 and − 550 [37]. The increase in Co nanoparticle size with increasing reduction temperature (as determined by XRD analysis) does not facilitate the exposure of Co^0. Meanwhile, the anchoring effect of the Al_2O_3 support limits the reduction of CoO on the catalyst surface. Therefore, a large amount of Co^{2+} existed in Co-Al-O-650 and − 700 [43]. Compared with those of Co-Al-O-500, the XPS signals of samples reduced at higher temperatures were shifted to higher binding energies, i.e., the chemical environment of Co^0 and Co^{2+} changed with increasing reduction temperature [57]. The offset was related to the strength of the interaction between the metal species and the support. Zhou et al. [37] reported that CoO can react with SiO_2 on the surface of KIT-6 to form Co_2SiO_4, which leads to a strong interaction between CoO and the KIT-6 support and thus makes it easier for the holes in the Co 3d orbital to accept electrons and increase the electron cloud density of this orbital. According to XRD analysis, no $CoAl_2O_4$ was generated, which indicated that the Co 3d outer electron cloud density and the shielding effect of the outer electrons on the inner electrons decreased [57]. As a result, the binding energy increased with increasing reduction temperature.

3.8. In situ DRIFTS

In order to gain further insights into the reaction mechanism and the

Table 2
Selected results of CO_2-TPD and XPS analysis.

Sample	nCO_2 (mmol g_{cat}^{-1})[a]		Content in fresh catalyst (%)		ΔE (eV)[b]	Content in spent catalyst (%)	
	α	β	Co^0	Co^{2+}		Co^0	Co^{2+}
Co-Al-O-500	0.67	1.27	45.4	54.6	15.8	63.0	37.0
Co-Al-O-550	0.64	1.17	50.6	49.4	15.8	63.5	36.5
Co-Al-O-600	0.60	2.30	61.6	38.4	15.7	70.1	29.9
Co-Al-O-650	0.52	1.90	55.2	44.8	15.9	64.6	35.4
Co-Al-O-700	0.15	1.60	50.5	49.5	15.9	66.1	33.9

[a] Calculated from CO_2-TPD profiles.
[b] ΔE = binding energy (Co $2p_{1/2}$) − binding energy (Co $2p_{3/2}$).

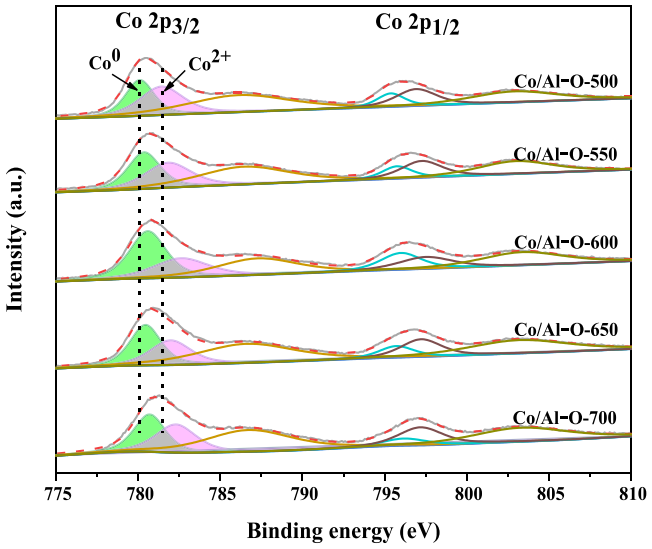

Fig. 8. Co 2p spectra of the prepared catalysts.

evolution of surface intermediates, the mechanism of Co-Al-O-600–promoted methanation was probed by *in situ* DRIFTS. Fig. 9 shows DRIFT spectra recorded in the region of 1000–2000 cm^{-1} after the adsorption of the reaction gas for different time over Co-Al-O-600 catalyst at 300 °C. The band of monodentate formate at 1363 cm^{-1} was stable and did not change with temperature, indicating that formate was an important intermediate of the methanation process [41]. With the adsorption time increased, the band of carbonate/bicarbonate species are distinctly observed at 1464, 1514, 1567 and 1630 cm^{-1} under test condition [58,59]. Concomitantly, the intensity of IR band for methane (1310 cm^{-1}) concomitantly improved, implying active sites increased with the reaction gas adsorption time.

It was generally believed the main process of methane formation is that CO_2 hydrogenated into formate firstly and converted into methoxy over supported catalysts [60]. Therefore, the content of formate on the catalyst is an important factor affecting the synthesis of methane. On the basis of *in situ* DRIFT spectra results, there is also a considerable amount of carbonate/bicarbonate species, indicated that methanation may not only occur through the formate pathway but carbonate/bicarbonate species are also important intermediates and can be hydrogenated into methane. As a consequence, high CO_2 conversion and CH_4 selectivity can be achieved simultaneously over Co-Al-O-600 catalyst.

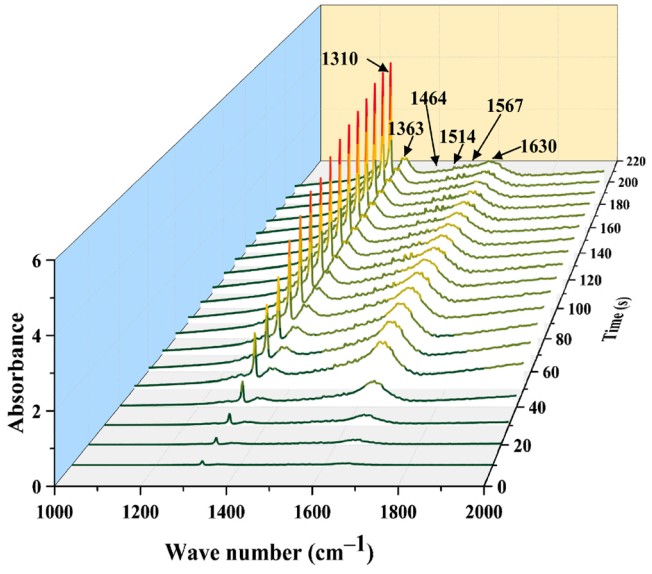

Fig. 9. *In situ* DRIFT spectra for CO_2 methanation over Co-Al-O-600 catalyst at 300 °C.

3.9. Catalytic activity tests

Fig. 10 presents the catalytic performance achieved by different

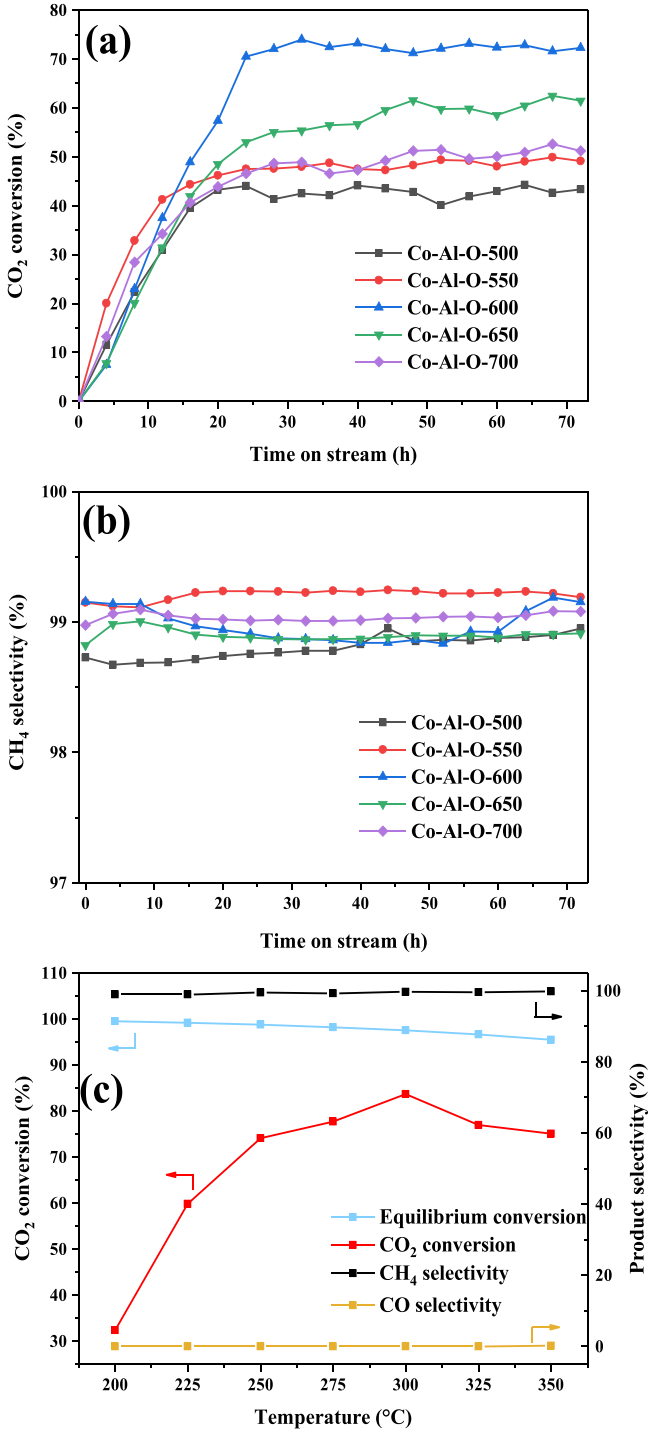

Fig. 10. (a,b) Effect of time on stream on CO_2 conversion and CH_4 selectivity at 250 °C for different catalysts. (c) Equilibrium conversion and effect of temperature on the maximal CO_2 conversion and CH_4 selectivity achieved over Co-Al-O-600 (The equilibrium conversion was calculated using a Gibbs free energy minimization simulation available in the Aspen Plus software from Aspen-Tech [61,62]).

catalysts, revealing that all samples showed high methanation activity, with CO_2 conversion following the order of Co-Al-O-600 > Co-Al-O-650 > Co-Al-O-700 > Co-Al-O-550 > Co-Al-O-500. The CH_4 selectivity of all samples was close to 100%, and no CO was detected. As shown in Fig. 10a and b, Co-Al-O-600 exhibited the highest CO_2 hydrogenation activity among the tested catalysts, achieving a CO_2 conversion of 74% and a CH_4 selectivity of 99% after a short induction period. For this catalyst, CO_2 conversion first increased with increasing reaction temperature to reach a maximum of 84% at 300 °C, which was close to equilibrium conversion and then slightly decreased, whereas CH_4 selectivity remained close to 100% at all temperatures (Fig. 10c). Higher reaction temperatures correspond to higher amounts of energy supplied to the reaction system and therefore promote the activation of CO_2 and H_2 and increase the frequency of collisions between reactant molecules. Thus, CO_2 conversion first increases with increasing reaction temperature. On the other hand, CO_2 methanation is an exothermic reaction and is limited by the thermodynamic equilibrium. Hence, high reaction temperatures are not conducive to methanation and promote the production of CO by the RWGS, as exemplified by the detection of ~0.1% CO at 350 °C. Therefore, CO_2 hydrogenation performance decreases at high reaction temperatures. Fig. S4 shows the turnover frequency (TOF) achieved by different catalysts, indicating Co-Al-O-600 exhibited the most efficient CO_2 conversion due to higher Co^0 content and moderate alkalinity on the surface. The TOF value of 9.76×10^{-4} s^{-1} over Co-Al-O-600 was much higher than that of 8.04×10^{-4} s^{-1} over Co-Al-O-500. With the reduction temperature increasing, more Co^0 content was achieved but the large Co crystalline size is not conducive to the exposure of corner and edge sites which have high CO_2 catalytic hydrogenation activity, leading to lower TOF values.

3.10. Durability test

The durability of Co-Al-O-600 was investigated at 300 °C because of the best performance (Fig. 11). After an initial stabilisation stage, this catalyst showed an approximately constant CO_2 conversion of 83%, while CH_4 selectivity was stable at nearly 100% during the entire reaction process. This result indicated the superior performance stability of Co-Al-O-600.

The origin of this high stability was probed by TGA (Fig. S5). The initial weight decrease below 200 °C was attributed to the loss of physically adsorbed water and some absorbed CO_2, and the subsequent gradual weight gain was ascribed to the oxidation of Co metal. The absence of further obvious weight loss indicated that no significant amounts of carbon were deposited on the spent catalyst. This excellent resistance to coking was attributed to moderate surface alkalinity, as revealed by CO_2-TPD measurements.

3.11. Characterisation of spent catalysts

Fig. 12 shows the XRD patterns of catalysts after 72-h operation at 250 °C. For all catalysts, the intensity of the Co metal peak significantly increased after operation, and the peaks of CoO became almost invisible. This result suggests that catalysts reduced at low temperatures experienced phase transitions during the reaction and were gradually reduced. The TPR peak corresponding to the reduction of mixed oxides spinels was centred at 693 °C, that is, the mixed Co-Al oxide cannot be completely activated at prepared temperatures. Furthermore, the presence of CoO in all samples which was ascribed to passivation process and not fully reduced was probably one of the reasons for the long stabilisation time observed for the initial reaction process. In addition, no peaks of deposited carbon were found for any spent catalyst, which was indicative of excellent resistance to coking. The XPS of spent catalysts indicated that the content of Co^0 significantly increased after the reaction, confirming the occurrence of phase transitions during the reaction process (Fig. S6 and Table 2).

Fig. 13 presents a SEM image of spent Co-Al-O-600 and the related EDS mappings, revealing that the high stability and activity of this catalyst were due to the retention of the original layered structure and the absence of metal aggregation. Moreover, Co, Al, and O remained highly dispersed after the reaction, i.e., the available metallic surface area did not markedly decrease. These results indicate that the layered support has a certain anchoring effect on active metals and restricts their migration and agglomeration to afford high durability and catalytic performance.

On the basis of above understanding, the activity and selectivity over Co-Al-O catalysts have been shown to be sensitive to the reduction temperature. With the reduction temperature increasing, Co species could be better reduced to expose more active sites. Nevertheless, the Co^0 species tended to agglomerate and layered structure of the catalyst was partly destroyed when the temperature was higher than 600 °C, as the XRD and SEM results showed. The higher Co^0/Co^{2+} atomic ratio and basic sites on the surface of Co-Al-O-600 catalyst contributed to a superior ability for the adsorption and activation of reactants at relatively a low temperature, which led to an efficiency reaction pathway via the

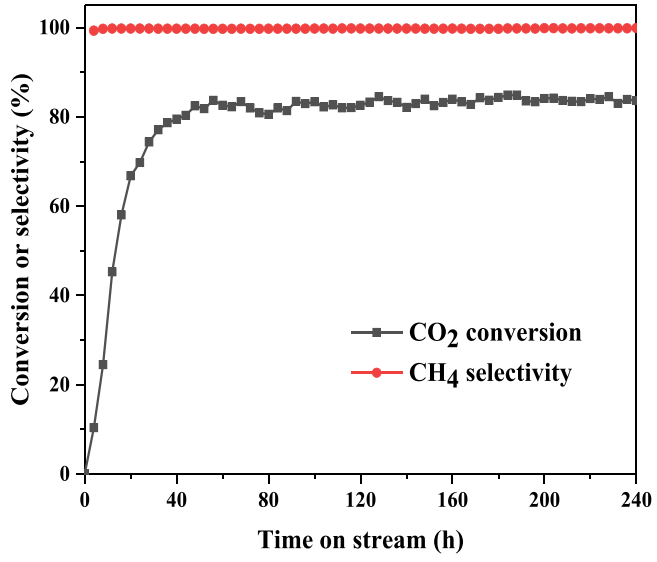

Fig. 11. Durability of the Co-Al-O-600 catalyst during CO_2 methanation at 300 °C.

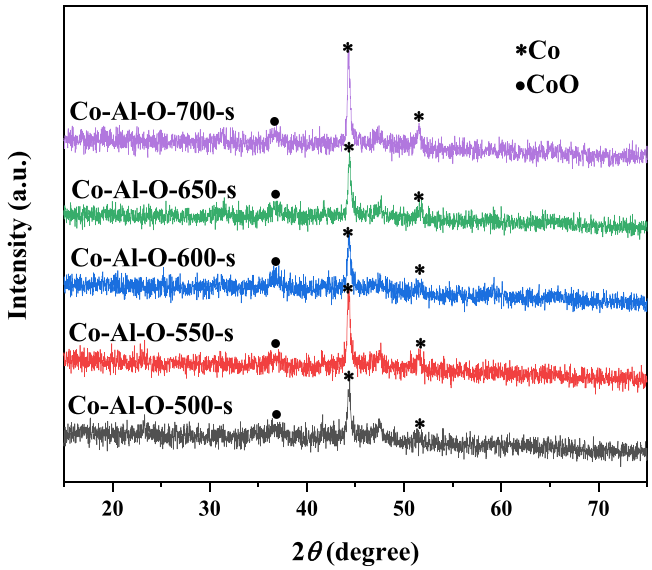

Fig. 12. XRD patterns of catalysts recorded after 72-h operation at 250 °C.

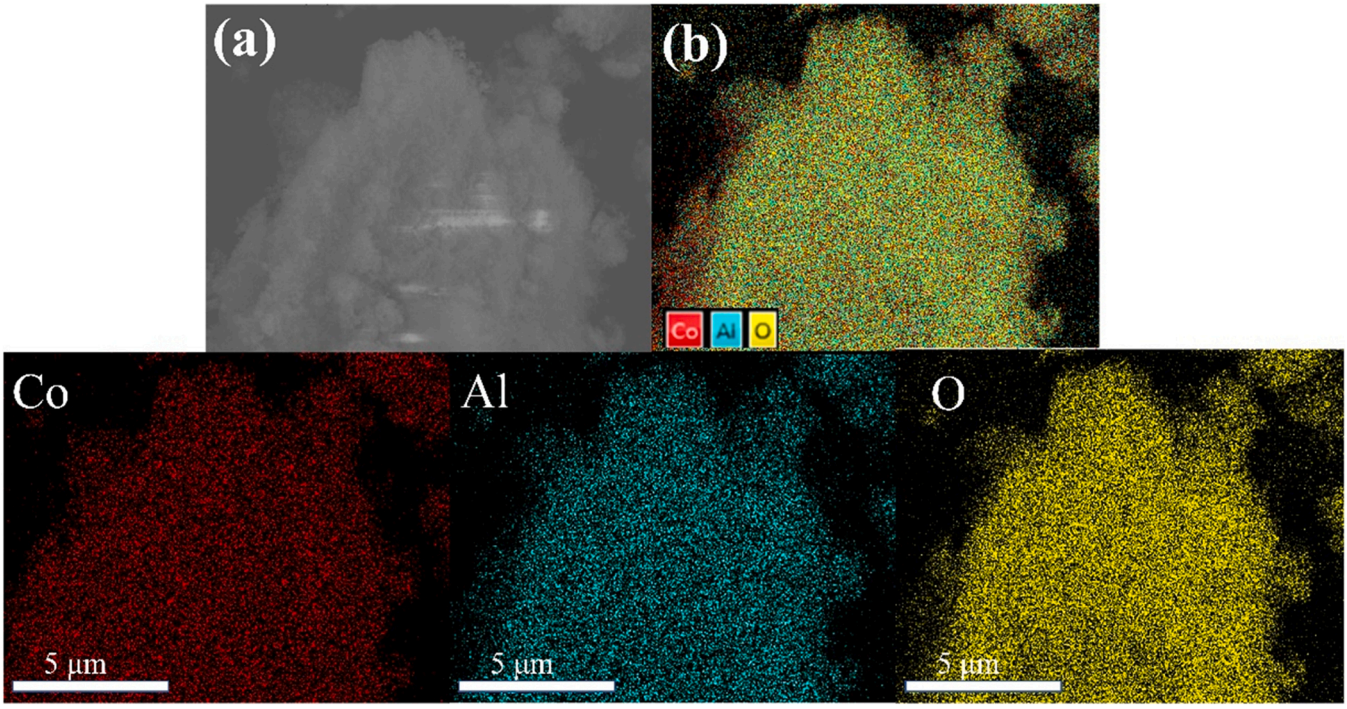

Fig. 13. SEM image of Co-Al-O-600 acquired after 72-h operation (a) and the corresponding elemental mappings (b).

formation of formates/carbonates species. Consequently, an excellent catalytic performance was achieved with CO_2 conversion of 74% and CH_4 selectivity of 99% at 250 °C, which was better than other Co-based catalysts reported elsewhere. Moreover, the catalyst remained stable for a long time on stream of 240 h and provided a reference for the design of low-temperature methanation catalysts in industry.

4. Conclusion

Layered Co-Al-O catalysts prepared by reducing Co-Al oxide derived from Co-Al LDH were used to promote CO_2 methanation at low temperatures. The reduction temperature had a significant impact on surface Co^0 content and CO_2 adsorption sites, showing a trend of first increasing and then decreasing with the reduction temperature increasing. The catalyst prepared at a reduction temperature of 600 °C exhibited the best performance, achieving a CO_2 conversion of 74% and a CH_4 selectivity of 99% at 250 °C. This high performance was ascribed to the high Co^0 content and more basic sites, which was considered to be effective for dissociation of H_2 and CO_2 adsorption, and was retained after a time on stream of 240 h. *In situ* DRIFTS indicated that formate and carbonate are essential intermediates produced during CO_2 methanation. At low reduction temperatures, Co^{2+} could not be completely reduced to active Co metal, whereas high reduction temperatures led to the aggregation of Co^0 and limited the exposure of corner and edge sites known to promote CO_2 hydrogenation. The present work provides a promising approach to develop high active Co-based catalyst for CO_2 methanation.

CRediT authorship contribution statement

Zhihao Liu: Methodology, Validation, Writing – original draft. **Xinhua Gao:** Conceptualization, Methodology, Validation, Funding acquisition, Writing – review & editing, Project administration. **Bo Liu:** Methodology, Validation. **Wenlong Song:** Methodology, Validation. **Qingxiang Ma:** Methodology, Validation. **Tian-sheng Zhao:** Conceptualization, Methodology, Validation, Funding acquisition. **Xu Wang:** Methodology. **Jong Wook Bae:** Methodology, Investigation. **Xingjun Zhang:** Validation. **Jianli Zhang:** Funding acquisition, Writing – review & editing, Project administration, Supervision.

Declaration of Competing Interest

The authors declare that they have no known competing financial interests or personal relationships that could have appeared to influence the work reported in this paper.

Acknowledgement

This work was financially supported in part by the National Natural Science Foundation of China (No. 21965029, No. 21968025), Innovation Leadership Program in Sciences and Technologies of Ningxia (2020GKLRLX09), Fourth Batch of Ningxia Youth Talents Supporting Program (TJGC2019022) and West Light Foundation of the Chinese Academy of Sciences (XAB2019AW02).

Appendix A. Supporting information

Supplementary data associated with this article can be found in the online version at doi:10.1016/j.apcatb.2022.121303.

References

[1] G.A. Meehl, W.M. Washington, W.D. Collins, J.M. Arblaster, A. Hu, L.E. Buja, W. G. Strand, H. Teng, How much more global warming and sea level rise? Science 307 (5716) (2005) 1769–1772.
[2] W. Wang, S. Wang, X. Ma, J. Gong, Recent advances in catalytic hydrogenation of carbon dioxide, Chem. Soc. Rev. 40 (7) (2011) 3703–3727.
[3] S. Saeidi, N. Amin, M. Rahimpour, Hydrogenation of CO_2 to value-added products—a review and potential future developments, J. CO2 Util. 5 (2014) 66–81.
[4] T. Bruhn, H. Naims, B. Olfe-Kräutlein, Separating the debate on CO_2 utilisation from carbon capture and storage, Environ. Sci. Policy 60 (2016) 38–43.
[5] L. Li, N. Zhao, W. Wei, Y. Sun, A review of research progress on CO_2 capture, storage, and utilization in Chinese Academy of Sciences, Fuel 108 (2013) 112–130.
[6] X. Yu, J. Zhang, X. Wang, Q. Ma, X. Gao, H. Xia, X. Lai, S. Fan, T.S. Zhao, Fischer-Tropsch synthesis over methyl modified Fe_2O_3@SiO_2 catalysts with low CO_2 selectivity, Appl. Catal. B: Environ. 232 (2018) 420–428.

[7] I. Dimitriou, P. García-Gutiérrez, R.H. Elder, R.M. Cuéllar-Franca, A. Azapagic, R. W.K. Allen, Carbon dioxide utilisation for production of transport fuels: process and economic analysis, Energy Environ. Sci. 8 (6) (2015) 1775–1789.

[8] W. Li, X. Nie, X. Jiang, A. Zhang, F. Ding, M. Liu, Z. Liu, X. Guo, C. Song, ZrO_2 support imparts superior activity and stability of Co catalysts for CO_2 methanation, Appl. Catal. B: Environ. 220 (2018) 397–408.

[9] J. Graciani, K. Mudiyanselage, F. Xu, A.E. Baber, J. Evans, S.D. Senanayake, D. J. Stacchiola, P. Liu, J. Hrbek, J. Fernández Sanz, J.A. Rodriguez, Highly active copper-ceria and copper-ceria-titania catalysts for methanol synthesis from CO_2, Science 345 (6196) (2014) 546–550.

[10] G. Centi, S. Perathoner, Opportunities and prospects in the chemical recycling of carbon dioxide to fuels, Catal. Today 148 (3–4) (2009) 191–205.

[11] M.D. Porosoff, X. Yang, J.A. Boscoboinik, J.G. Chen, Molybdenum carbide as alternative catalysts to precious metals for highly selective reduction of CO_2 to CO, Angew. Chem. Int. Ed. 53 (26) (2014) 6705–6709.

[12] M. Younas, L. Loong Kong, M.J.K. Bashir, H. Nadeem, A. Shehzad, S. Sethupathi, Recent advancements, fundamental challenges, and opportunities in catalytic methanation of CO_2, Energy Fuels 30 (11) (2016) 8815–8831.

[13] J. Chen, X. Wang, D. Wu, J. Zhang, Q. Ma, X. Gao, X. Lai, H. Xia, S. Fan, T.S. Zhao, Hydrogenation of CO_2 to light olefins on CuZnZr@(Zn-)SAPO-34 catalysts: Strategy for product distribution, Fuel 239 (2019) 44–52.

[14] W.J. Lee, C. Li, H. Prajitno, J. Yoo, J. Patel, Y. Yang, S. Lim, Recent trend in thermal catalytic low temperature CO_2 methanation: a critical review, Catal. Today 368 (2021) 2–19.

[15] M. Götz, J. Lefebvre, F. Mörs, A. McDaniel Koch, F. Graf, S. Bajohr, R. Reimert, T. Kolb, Renewable Power-to-Gas: a technological and economic review, Renew. Energy 85 (2016) 1371–1390.

[16] J. Kirchner, J.K. Anolleck, H. Lösch, S. Kureti, Methanation of CO_2 on iron based catalysts, Appl. Catal. B Environ. 223 (2018) 47–59.

[17] J. Gao, Y. Wang, Y. Ping, D. Hu, G. Xu, F. Gu, F. Su, A thermodynamic analysis of methanation reactions of carbon oxides for the production of synthetic natural gas, RSC Adv. 2 (6) (2012) 2358–2368.

[18] X. Nie, H. Wang, W. Li, Y. Chen, X. Guo, C. Song, DFT insight into the support effect on the adsorption and activation of key species over Co catalysts for CO_2 methanation, J. CO2 Util. 24 (2018) 99–111.

[19] G. Zhou, T. Wu, H. Xie, X. Zheng, Effects of structure on the carbon dioxide methanation performance of Co-based catalysts, Int. J. Hydrog. Energy 38 (24) (2013) 10012–10018.

[20] S. He, C. Li, H. Chen, D. Su, B. Zhang, X. Cao, B. Wang, M. Wei, D.G. Evans, X. Duan, A surface defect-promoted Ni nanocatalyst with simultaneously enhanced activity and stability, Chem. Mater. 25 (7) (2013) 1040–1046.

[21] P. Riani, I. Valsamakis, T. Cavattoni, V. Sanchez Escribano, G. Busca, G. Garbarino, Ni/SiO_2-Al_2O_3 catalysts for CO_2 methanation: effect of La_2O_3 addition[J], Appl. Catal. B: Environ. 284 (2021), 119697.

[22] A. Govender, D. Curulla Ferré, J. Niemantsverdriet, A density functional theory study on the effect of zero-point energy corrections on the methanation profile on Fe (100), ChemPhysChem 13 (6) (2012) 1591–1596.

[23] K. Manthiram, B. Beberwyck, A. Alivisatos, Enhanced electrochemical methanation of carbon dioxide with a dispersible nanoscale copper catalyst, J. Am. Chem. Soc. 136 (38) (2014) 13319–13325.

[24] A.M. Abdel-Mageed, K. Wiese, A. Hauble, J. Bansmann, J. Rabeah, M. Parlinska-Wojtan, A. Brückner, R.J. Behm, Steering the selectivity in CO_2 reduction on highly active Ru/TiO_2 catalysts: support particle size effects, J. Catal. 401 (2021) 160–173.

[25] A. Karelovic, P. Ruiz, CO_2 hydrogenation at low temperature over Rh/γ-Al_2O_3 catalysts: effect of the metal particle size on catalytic performances and reaction mechanism, Appl. Catal. B: Environ. 113–114 (2012) 237–249.

[26] L. Luo, M. Wang, Y. Cui, Z. Chen, J. Wu, Y. Cao, J. Luo, Y. Dai, W.X. Li, J. Bao, J. Zeng, Surface iron species in palladium-iron intermetallic nanocrystals that promote and stabilize CO_2 methanation, Angew. Chem. Int. Ed. 132 (34) (2020) 14434–14442.

[27] C.G. Visconti, M. Martinelli, L. Falbo, L. Fratalocchi, L. Lietti, CO_2 hydrogenation to hydrocarbons over Co and Fe-based Fischer-Tropsch catalysts, Catal. Today 277 (2016) 161–170.

[28] C.G. Visconti, M. Martinelli, L. Falbo, L. Fratalocchi, L. Lietti, CO_2 hydrogenation to hydrocarbons over Co and Fe-based Fischer-Tropsch catalysts, Catal. Today 277 (2016) 161–170.

[29] S. Abate, K. Barbera, E. Giglio, F. Deorsola, S. Bensaid, S. Perathoner, R. Pirone, G. Centi, Synthesis, characterization, and activity pattern of Ni–Al hydrotalcite catalysts in CO_2 methanation, Ind. Eng. Chem. Res. 55 (30) (2016) 8299–8308.

[30] G. Weatherbee, C. Bartholomew, Hydrogenation of CO_2 on group VIII metals: IV. Specific activities and selectivities of silica-supported Co, Fe, and Ru, J. Catal. 87 (2) (1984) 352–362.

[31] J. Ashok, M. Ang, S. Kawi, Enhanced activity of CO_2 methanation over Ni/CeO_2-ZrO_2 catalysts: influence of preparation methods, Catal. Today 281 (2017) 304–311.

[32] R. Razzaq, C. Li, M. Usman, K. Suzuki, S. Zhang, A highly active and stable Co_4N/γ-Al_2O_3 catalyst for CO and CO_2 methanation to produce synthetic natural gas (SNG), Chem. Eng. J. 262 (2015) 1090–1098.

[33] G. Zhou, T. Wu, H. Zhang, H. Xie, Y. Feng, Carbon dioxide methanation on ordered mesoporous Co/KIT-6 catalyst, Chem. Eng. Commun. 201 (2) (2014) 233–240.

[34] D. dos Santos Lima, Y. Dias, O. Perez-Lopez, CO_2 methanation over Ni–Al and Co–Al LDH-derived catalysts: the role of basicity, Sustain. Energy Fuels 4 (11) (2020) 5747–5756.

[35] J. Kwak, L. Kovarik, J. Szanyi, Heterogeneous catalysis on atomically dispersed supported metals: CO_2 reduction on multifunctional Pd catalysts, ACS Catal. 3 (9) (2013) 2094–2100.

[36] Y. Liu, K. Fang, J. Chen, Y. Sun, Effect of pore size on the performance of mesoporous zirconia-supported cobalt Fischer-Tropsch catalysts, Green. Chem. 9 (6) (2007) 611–615.

[37] H. Liu, S. Xu, G. Zhou, G. Huang, S. Huang, K. Xiong, CO_2 hydrogenation to methane over Co/KIT-6 catalyst: effect of reduction temperature, Chem. Eng. J. 351 (2018) 65–73.

[38] X. Wang, H. Shi, J.H. Kwak, J. Szanyi, Mechanism of CO_2 hydrogenation on Pd/Al_2O_3 catalysts: kinetics and transient DRIFTS-MS studies, ACS Catal. 5 (11) (2015) 6337–6349.

[39] X. Gao, C. Jin, D. Llusia, Y. Li, Recent advances in methanation catalysts for the production of synthetic natural gas, RSC Adv. 5 (29) (2015) 22759–22776.

[40] X. Guo, Z. Peng, M. Hu, C. Zuo, A. Traitangwong, V. Meeyoo, C. Li, S. Zhang, Highly active Ni-based catalyst derived from double hydroxides precursor for low temperature CO_2 methanation, Ind. Eng. Chem. Res. 57 (28) (2018) 9102–9111.

[41] J.A. Gursky, S.D. Blough, C. Luna, C. Gomez, A.N. Luevano, E.A. Gardner, Particle-particle interactions between layered double hydroxide nanoparticles, J. Am. Chem. Soc. 128 (26) (2006) 8376–8377.

[42] P.J. Sideris, U.G. Nielsen, Z. Gan, C.P. Grey, Mg/Al ordering in layered double hydroxides revealed by multinuclear NMR spectroscopy, Science 321 (5885) (2008) 113–117.

[43] C. Li, L. Wang, M. Wei, D.G. Evans, X. Duan, Large oriented mesoporous self-supporting Ni–Al oxide films derived from layered double hydroxide precursors, J. Mater. Chem. 18 (23) (2008) 2666–2672.

[44] D. Wierzbicki, R. Baran, R. Dębek, M. Motak, M.E. Gálvez, T. Grzybek, P. Da Costa, P. Glatzel, Examination of the influence of La promotion on Ni state in hydrotalcite-derived catalysts under CO_2 methanation reaction conditions: operando X-ray absorption and emission spectroscopy investigation[J], Appl. Catal. B Environ. 232 (2018) 409–419.

[45] Q. Xu, X. Xu, G. Fan, et al., Unveiling the roles of Fe-Co interactions over ternary spinel-type $ZnCo_xFe_{2-x}O_4$ catalysts for highly efficient CO_2 hydrogenation to produce light olefins, J. Catal. 400 (2021) 355–366.

[46] H. Liu, S. Xu, G. Zhou, K. Xiong, Z. Jiao, S. Wang, CO_2 hydrogenation to methane over Co/KIT-6 catalysts: effect of Co content[J], Fuel 217 (2018) 570–576.

[47] G. Zhou, H. Liu, K. Cui, H. Xie, Z. Jiao, G. Zhang, K. Xiong, X. Zheng, Methanation of carbon dioxide over Ni/CeO_2 catalysts: effects of support CeO_2 structure, Int. J. Hydrog. Energy 42 (25) (2017) 16108–16117.

[48] Y. Shan, K. Liew, J. Li, Effect of silylation of SBA-15 on its supported cobalt catalysts for Fischer-Tropsch synthesis, Chin. J. Catal. 30 (11) (2009) 1091–1095.

[49] F. Zhang, B. Lu, P. Sun, Co-promoted Ni nanocatalysts derived from NiCoAl-LDHs for low temperature CO_2 methanation, Catalysts 11 (1) (2021) 121.

[50] G. Zhou, H. Liu, Y. Xing, S. Xu, H. Xie, K. Xiong, CO_2 hydrogenation to methane over mesoporous Co/SiO_2 catalysts: effect of structure, J. CO2 Util. 26 (2018) 221–229.

[51] L. Zardin, O. Perez-Lopez, Hydrogen production by methane decomposition over Co-Al mixed oxides derived from hydrotalcites: effect of the catalyst activation with H_2 or CH_4, Int. J. Hydrog. Energy 42 (12) (2017) 7895–7907.

[52] C. Calgaro, O. Perez-Lopez, Decomposition of methane over $Co_{3-x}Al_xO_4$ (x=0–2) coprecipitated catalysts. The role of Co phases in the activity and stability, Int. J. Hydrog. Energy 42 (50) (2017) 29756–29772.

[53] M. Tan, X. Wang, X. Wang, X. Zou, W. Ding, X. Lu, Influence of calcination temperature on textural and structural properties, reducibility, and catalytic behavior of mesoporous γ-alumina-supported Ni–Mg oxides by one-pot template-free route, J. Catal. 329 (2015) 151–166.

[54] X. Jia, X. Zhang, N. Rui, X. Hu, C. Liu, Structural effect of Ni/ZrO_2 catalyst on CO_2 methanation with enhanced activity, Appl. Catal. B Environ. 244 (2019) 159–169.

[55] L. Jin, Y. Li, P. Lin, H. Hu, CO_2 reforming of methane on Ni/γ-Al_2O_3 catalyst prepared by dielectric barrier discharge hydrogen plasma, Int. J. Hydrog. Energy 39 (11) (2014) 5756–5763.

[56] Y. Yao, Y. Cai, G. Wu, F. Wei, X. Li, H. Chen, S. Wang, Sulfate radicals induced from peroxymonosulfate by cobalt manganese oxides ($Co_xMn_{3-x}O4$) for Fenton-like reaction in water, J. Hazard. Mater. 296 (2015) 128–137.

[57] S.S. Bhoware, S. Shylesh, K.R. Kamble, A.P. Singh, Cobalt-containing hexagonal mesoporous molecular sieves (Co-HMS): synthesis, characterization and catalytic activity in the oxidation reaction of ethylbenzene, J. Mol. Catal. A Chem. 255 (1–2) (2006) 123–130.

[58] C. Zhou, J. Shi, W. Zhou, K. Cheng, Q. Zhang, J. Kang, Y. Wang, Highly active ZnO-ZrO_2 aerogels integrated with H-ZSM-5 for aromatics synthesis from carbon dioxide, ACS Catal. 10 (1) (2019) 302–310.

[59] M. Zhu, P. Tian, X. Cao, J. Chen, T. Pu, B. Shi, J. Xu, J. Moon, Z. Wu, Y.F. Han, Vacancy engineering of the nickel-based catalysts for enhanced CO_2 methanation, Appl. Catal. B Environ. 282 (2021), 119561.

[60] Y. Ma, J. Liu, M. Chu, J. Yue, Y. Cui, G. Xu, Cooperation between active metal and basic support in Ni-based catalyst for low-temperature CO_2 methanation, Catal. Lett. 150 (5) (2020) 1418–1426.

[61] J. Gao, Y. Wang, Y. Ping, D. Hu, G. Xu, F. Gu, F. Su, A thermodynamic analysis of methanation reactions of carbon oxides for the production of synthetic natural gas, RSC Adv. 2 (6) (2012) 2358–2368.

[62] C.V. Miguel, M.A. Soria, A. Mendes, L.M. Madeira, Direct CO_2 hydrogenation to methane or methanol from post-combustion exhaust streams–a thermodynamic study, J. Nat. Gas. Sci. Eng. 22 (2015) 1–8.